Tectonophysics 663 (2015) 19–32

Contents lists available at ScienceDirect

Tectonophysics

journal homepage: www.elsevier.com/locate/tecto

Relief and drainage evolution during the exhumation of the Sierra Nevada (SE Spain): Is denudation keeping pace with uplift?

J.M. Azañón [a,b,*], J.P. Galve [a], J.V. Pérez-Peña [a,c], F. Giaconia [a], R. Carvajal [a], G. Booth-Rea [a,b], A. Jabaloy [a], M. Vázquez [d,e], A. Azor [a], F.J. Roldán [f]

[a] Departamento de Geodinámica, Campus de Fuentenueva, Universidad de Granada, 18071 Granada, Spain
[b] Instituto Andaluz de Ciencias de la Tierra, CSIC-UGR, Avd. Palmeras, 4, Armilla, Granada, Spain
[c] Instituto Andaluz de Geofísica, Campus Universitario de Cartuja, Universidad de Granada, 18071 Granada, Spain
[d] Andean Geothermal Center of Excellence (CEGA), Universidad de Chile, Santiago, Chile
[e] Department of Geology, Universidad de Chile, Santiago, Chile
[f] Instituto Geológico y Minero de España, Urb Alcázar del Genil, 4 Edf. Zulema bajo, Granada, Spain

ARTICLE INFO

Article history:
Received 26 December 2014
Received in revised form 4 May 2015
Accepted 13 June 2015
Available online 27 June 2015

Keywords:
Denudation rates
Unroofing processes
Drainage network analysis
Uplift pattern mapping

ABSTRACT

We have performed a geomorphic analysis of the Sierra Nevada, the highest range of the Betic Cordillera (SE Spain), with the aim to elucidate its late Miocene to present-day exhumation history. The qualitative and quantitative analysis is based on filtered topography, local relief, swath-profile analysis, anomalies on stream orientation, bulk erosion volume, hypsometry, and steepness index (k_{sn}). All these parameters are intimately linked to river incision and development of drainage pattern, having been calculated to assess the role of folding and faulting on the evolution of the Sierra Nevada. Moreover, uplift rates in the core of the Sierra Nevada have been deduced from an extrapolation of the position of Late Tortonian to Pliocene coastline deposits. These data have been compared to apatite (U–Th)/He, fission-track and ^{10}Be cosmogenic data from SE Spain in order to evaluate the consistency among uplift, thermal histories and denudation rates. Our preferred tectonic scenario is one that favors fast exhumation of the western Sierra Nevada in a NW–SE overall compressive setting produced by the convergence between the Nubia and Africa plates. Sub-perpendicular to this compression, a westward 4 mm/year extensional hanging-wall displacement promotes uplift and unroofing of the western part of Sierra Nevada.

1. Introduction

In orogenic areas with low to moderate tectonic activity, landscape analysis provides one of the best approaches for characterizing recent mountain belt evolution (e.g., Molin et al., 2004; Dumont et al., 2005; Necea et al., 2005). This analysis combined with radiometric techniques provides quantitative key insights on the spatial and temporal pattern of denudation and uplift of the relief (e.g., Burbank et al., 1996; Whipple, 2004).

The estimation of denudation and uplift rates must follow a multidisciplinary approach, since very diverse processes can produce similar results (e.g., Burbank and Anderson, 2013). In this regard, the assimilation of denudation rates to surface uplift rates related to tectonic movements is especially illustrative. In fact, besides tectonics, a number of factors related to fluvial dynamics can be responsible for river entrenchment, namely discharge variations, bed load decrease, and base level lowering. Some of these factors may be climatically controlled, while others are mostly controlled by river-bed lithology (Dethier et al., 2014).

For landscapes in steady state conditions river incision is commonly argued to regulate the overall rate of erosion (Burbank and Anderson, 2013). Power law scaling rules for river in dynamic equilibrium can be used to determine rock uplift rates (Wobus et al., 2006; Kirby and Whipple, 2012; Whipple et al., 2013; Burbank and Anderson, 2013; Bellin et al., 2014; Scotti et al., 2014). However, transient landscapes responding to changes in the rate of base-level fall, tectonic uplift and/or precipitation may generate convex rivers for which these assumed scaling rules may be inappropriate (Whittaker et al., 2007). Therefore, attribution of river incision to active tectonics is not straightforward and requires determining the right landscape evolution model.

Long-term topographic steady-state has been suggested for some active mountain ranges worldwide; the Central Range of Taiwan (Whipple, 2001), the Central and Western Alps (Wittmann et al., 2007), the Northern Apennines (Cyr and Granger, 2008), and the Olympic Mountains (Pazzaglia and Brandon, 2001), whereas transient landscapes often are found in young mountain topography (Densmore et al., 2007) or related to increases in tectonic uplift (Whittaker et al., 2007; Harkins et al., 2007).

* Corresponding author.
E-mail address: jazanon@ugr.es (J.M. Azañón).

http://dx.doi.org/10.1016/j.tecto.2015.06.015
0040-1951/

In steady-state mountain belts, incised rivers and active landsliding could be considered, in a first approach, as topographic expressions of high denudation rates due to uplift induced by active tectonics. This may be accompanied by a perturbation of the drainage network causing wind and water gaps (e.g., Babault et al., 2012) or by landslide erosion (Larsen and Montgomery, 2012). In this sense, drainage network analysis and stream incision estimations have become one of the classical issues concerning tectonic geomorphology (e.g., Burbank et al., 1996; Azor et al., 2002; van der Beek et al., 2002; Wegmann and Pazzaglia, 2002; Dadson et al., 2003; Zhang et al., 2004; Pérez-Peña et al., 2010).

The aim of this contribution is twofold: first, to characterize qualitatively the spatial pattern of uplift and subsidence in an area of moderate-tectonic activity on the basis of a number of qualitative and quantitative tools, including topographic metrics of hillslope, catchment and channel morphology; second, to derive approximate denudation and uplift rates from morphometric indexes and to compare them

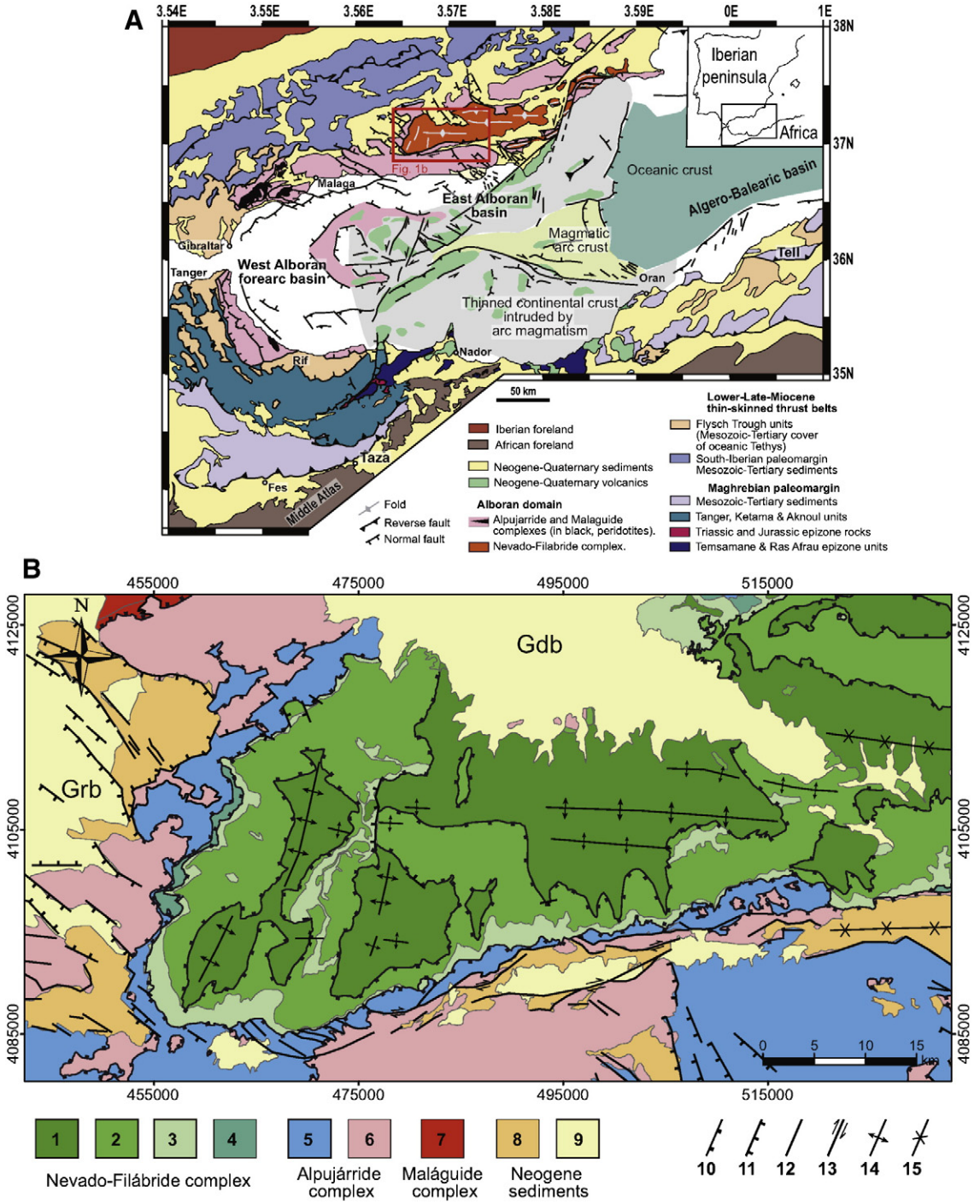

Fig. 1. A) Simplified geological map showing the tectonic domains of the Gibraltar Arc and the Alboran and Algero–Balearic basins [modified from Comas et al., 1999; Booth-Rea et al., 2003; Giaconia et al., 2012]. The inset shows the main tectonic structures of the study area together with sedimentary basins and antiformal ridges. B) Litho-structural map of the study area (modified from Martínez-Martínez, 2006). *Nevado Filabride complex*: (1) Ragua unit, (2) and (3) Calar–Alto unit, Palaeozoic and Permo–Triassic rocks, respectively, and (4) Bédar–Macael unit. *Alpujarride complex*: (5) Lújar–Gador unit and (6) upper Alpujárride units. *Malaguide complex*: (7) undifferentiated. *Neogene sediments*: (8) Miocene and (9) Pliocene to Quaternary. 10) Low-angle inactive normal fault, 11) high angle normal fault, 12) high angle normal fault (undifferentiated), 13) strike-slip fault, 14) anticline, and 15 syncline. Gdb: Guadix basin and Grb: Granada basin.

with previous published data. The study area is focused on the Sierra Nevada, i.e., the highest mountain range of the Betic Cordillera (SE Spain). This range is in the central portion of the 300-km-wide tectonic zone between Eurasia and Africa that accommodates a present-day convergence rate of 4–5 mm/year (DeMets et al., 1990, 1994). Previous studies have confirmed the moderate-deformation rate of specific structures in this sector of the Betics (Masana et al., 2004; Morales et al., 2013). Our study evaluates if (1) there is equilibrium between denudation and uplift processes and (2) the estimated rates are consistent to the regional stress field and structural framework.

2. Geologic and tectonic setting

2.1. The Betic–Rif cordillera: the western termination of the Alpine orogen

The Betic–Rif cordillera (Fig. 1) forms the western termination of the peri-Mediterranean Alpine orogen, being related on a broad scale to the northwest-directed dextrally oblique convergence between Africa and Iberia (DeMets et al., 2010; Koulali et al., 2011; Platt et al., 2013). The kinematic picture of this orogenic belt is rather complicated because of the presence of a continental micro-plate that has migrated westwards, colliding in Eocene–early Oligocene times with the margins of southern Iberia and northern Africa, thus forming the arcuate Gibraltar arc system (Balanyá and García-Dueñas, 1987; DeMets et al., 1994; Lonergan, 1993; Platt et al., 2005). Thus, the Betic–Rif cordillera is made up of two external zones (the South Iberian margin in Spain and the Maghrebian margin in northern Morocco) with one internal zone in-between (the so-called Alborán Domain). The Alborán Domain is formed by several complexes that are distinguished by their stratigraphy, degree of metamorphism, and structural position (e.g., Booth-Rea et al., 2004, 2005). The early compressional tectono-metamorphic evolution of the Alborán Domain is partially obliterated by pervasive extensional tectonics, which occurred since Early–Middle Miocene times (e.g., Platt and Vissers, 1989; García-Dueñas et al., 1992; Lonergan and Platt, 1995; Martínez-Martínez and Azañón, 1997; Platt et al., 2013). This extension is responsible for ductile shear zones and low- and high-angle normal faults, as well as for the initial development of Neogene–Quaternary sedimentary basins. The largest of these sedimentary basins is the Alborán Sea (Watts et al., 1993; Comas et al., 1999), which was formed over the metamorphic rocks of the internal zone, separating the Rif in Northern Morocco from the Betics in Southern Spain (Fig. 1). The extensional tectonics seems to have occurred coevally with N–S oriented compressional structures also active since the Late Miocene and responsible for large-scale E–W oriented folds (Martínez-Martínez et al., 2002). These folds are responsible for the most outstanding topographic features in the internal zone of the Betic Cordillera: the antiforms coincide with the main ranges, which, thus, can be said to be antiformal ridges, while the synforms coincide with Neogene–Quaternary sedimentary basins (Fig. 1).

2.2. Exhumation of the Sierra Nevada in the last 15–18 Ma

The Sierra Nevada mountain range (Fig. 1) is formed by metamorphic rocks belonging to the Nevado–Filabride Complex, which has undergone a HP metamorphism of low to moderate temperature dated at 15–18 Ma (U–Pb ages on metamorphic zircons, (Sánchez-Vizcaino et al., 2002; Gómez-Pugnaire et al., 2012, and Lu–Hf ages from garnets in eclogites, Platt et al., 2006). After continental subduction at depths below 50 km, the Nevado–Filabride Complex was rapidly exhumed to shallow crustal levels, reaching the surface at 12–8 Ma (Johnson et al., 1997; Vázquez et al., 2011). Recently, Behr and Platt (2012) have proposed a two-fold exhumation model in a subduction channel. Actually, these authors claim that the Nevado–Filabride Complex was exhumed in the second stage of their model by a low-angle detachment fault rooted in the middle crust that produced the final exhumation with a westwards mean slip rate around 5 mm/year (Behr and Platt, 2012).

Major detachments and associated high-angle faults have a critical role in the most recent exhumation of the Nevado–Filabride Complex. Thus, this complex is separated from the overlying Alpujarride Complex by a detachment fault with brittle fault rocks in the hanging wall and mylonitic rocks in the footwall (Galindo-Zaldívar et al., 1989; Jabaloy et al., 1992; Visser et al., 1995; Martínez-Martínez et al., 2004). On the other hand, the western border of the Sierra Nevada is bounded by NW–SE striking normal faults (Fig. 1) that bound the sediments of the Neogene–Quaternary Granada sedimentary basin. These faults clearly indicate activity in Quaternary times, as deduced from seismicity and deformed Pleistocene–Holocene alluvial fans (Calvache and Viseras, 1997; Alfaro et al., 2001; Viseras et al., 2003). Some authors have proposed Quaternary slip rates of 0.6–0.8 mm/year for these faults (Sanz de Galdeano, 1996).

Coeval with the extensional structures, large-scale open antiformal folds have favored the exhumation of the whole extent of the Nevado–Filabride Complex outcropping in the Sierra Nevada. Galindo-Zaldívar et al. (2003) considered the antiformal ridge related to a blind-thrust buried under the northern E–W oriented mountain front of the Sierra Nevada, while the normal faults would be coeval and related to extension sub-perpendicular to the NNW–SSE axis of maximum shortening (Africa–Iberia present-day vector of convergence). However, Martínez-Martínez et al. (2002) proposed that the present-day topography of the Sierra Nevada is due to the interference of two orthogonal sets of Miocene–Pliocene, large-scale open folds trending roughly E–W and NNE–SSW. They suggested that the NNE–SSW folds were generated by a rolling-hinge mechanism, while the E–W folds were formed by shortening perpendicular to the direction of extension (Martínez-Martínez et al., 2002, 2004).

The northern and southern borders of the Sierra Nevada present very different tectonic activity (Pérez-Peña et al., 2010). The southern border is bounded by a WSW–ENE sub-vertical dextral strike-slip fault zone that has been active since the Miocene (Martínez-Martínez et al., 2006). On the contrary, the northern mountain front corresponds to the northern limb of an E–W fold, with the Neogene–Quaternary sediments of the Guadix–Baza basin unconformably overlaying the metamorphic rocks of the Sierra Nevada (Azañón et al., 2006; Pérez-Peña et al., 2009c; Sanz de Galdeano et al., 2012).

2.3. Denudation and uplift rates in the central and eastern Betics

Zircon fission-track (ZFT) and Apatite fission-track (AFT) data show that the Eastern parts of the Betics were exhumed earlier than the Central part (Johnson, 1997; Johnson et al., 1997; Reinhardt et al., 2007; Clark and Dempster, 2009; Vázquez et al., 2011). On the other hand, minimum denudation rates derived from these data range between 500–1800 m Ma^{-1} in the western Sierra Nevada (Johnson, 1997; Reinhardt et al., 2007; Vázquez et al., 2011). Johnson (1997) found that the AFT ages from the western Sierra Nevada are negatively correlated with their elevation and deduced a complex denudation history. This author proposed a first initial phase of tectonic denudation corresponding to the previously mentioned Tortonian to Messinian tectonic unroofing of the Nevado–Filabride complex, followed by a younger rapid cooling stage at around 5–3 Ma (Pliocene).

Concerning estimations derived from ^{10}Be concentrations on alluvial quartz, Bellin et al. (2014) determine very recent denudation rates for several catchments in the eastern Betics at time-scales of 103–105 years. They found relatively low denudation rates, though with a large variation (64 ± 54 m Ma^{-1}). Bellin et al. (2014) also indicate the consistence between these values and the uplift rates derived from uplifted marine deposits and fission tracks ages, which indicate a steady-state topography where rock uplift is balanced by denudation in the eastern Betics. By contrast, in the central Betics, data from ^{10}Be concentrations on alluvial sediments are limited to a single catchment in the western termination of the Sierra Nevada. The catchment-wide denudation rates were estimated in 1600 m Ma^{-1} (Reinhardt et al., 2007).

However, these very high rates could be explained by the progression of the incision wave due to the recent activity of an important normal fault that controls the local base level of this catchment (Padul–Nigüelas fault) (Reinhardt et al., 2007). The highest denudation rates calculated by Bellin et al. (2014) also coincide with catchments influenced by active faulting.

The most useful information on uplift rates in the Betics comes from the data compiled by Braga et al. (2003). These authors calculated uplift rates from the elevation of tectonically raised coastal deposits of known age. Thus, they estimated long-term average uplift rates from Late Tortonian to present-day of up to 0.28 mm/year (Sierra de Gádor). All these values lie well below denudation rates estimated by using fission-track methods, but they are coherent with the catchment-wide ^{10}Be-derived denudation rates of Bellin et al. (2014). The main limitation of the long-term rates is the spatial distribution of the data, since the deposits have only been preserved around the mountain ranges and there is no information in the high mountain areas. To sum up, the recent uplift and exhumation history of the central and eastern Betics is poorly constrained and several tentative models of exhumation have been proposed. Changes over time in cooling and denudation rates as well as potential differences in the exhumation history between diverse sectors of the Cordillera should be confirmed with new studies and radiometric age determinations. In this work, we assume that hillslope and channel morphology of the rivers exert a first order control on denudation rates and, therefore, could be excellent tools to investigate the apparent denudation rate differences between the Eastern and Central Betics. Accordingly, if the Betic Cordillera is a transient landscape or conversely the orogen is a steady-state topography are topics of current debate that can be solved by analyzing the relationships between uplift and denudation histories.

3. Methodology

We have applied diverse landscape analysis techniques that include local relief and minimum bulk erosion (E_{bulk}) estimation, swath profiles and catchment asymmetry evaluation, hypsometric analysis and normalized steepness index. The results of these methods have been contrasted with the patterns recognized in the drainage network. This qualitative assessment was completed by two additional analyses: (1) estimation of denudation rates on the basis of the correlation between the normalized steepness index and ^{10}Be-derived denudation rates; and (2) mapping the spatial pattern of uplift rates according to the data compiled by Braga et al. (2003).

3.1. Relief analysis

3.1.1. Local relief and swath profiles

In order to analyze the spatial variation of fluvial dissection along the Sierra Nevada, we have performed swath profiles and extracted the local relief. We followed the general approach proposed by Molin et al. (2004) to estimate the local relief, computing the remaining residual topography between a relief envelope and sub-envelope. The relief envelope is the upper surface that connects ridges and peaks, while the relief sub-envelope is the lower surface that link valley bottoms. These surfaces were derived from a smoothed model of the topography that represents the mountain range removing the lateral valleys.

To study the relief pattern of the Sierra Nevada, we have obtained six swath profiles across the mountain range: a W–E longitudinal profile, three N–S transversal profiles, and two oblique profiles in the western termination oriented SW–NE and NW–SE. All the swath profiles are 6 km wide and they have been generated by sampling elevation values along six parallel lines spaced 1 km. Maximum, minimum and mean elevation, as well as local relief (maximum minus minimum elevation) were projected into the plane of the profiles (Masek et al., 1994).

3.1.2. Hypsometric analysis

The hypsometric curve and the hypsometric integral (HI) are valuable tools for characterizing topography because they are correlated with the erosional stage of the landscape (Strahler, 1952; Willgoose and Hancock, 1998; Pérez-Peña et al., 2009a,b). In this work, we have followed the methodology proposed by Pérez-Peña et al. (2009b) to spatially analyze hypsometry. This methodology computes HI values for regular squares instead of values for basins and sub-basins, and then applies spatial-autocorrelation techniques to recognize possible spatial patterns. Since we did not use drainage basins, HI values do not strictly represent a measure of dissection but instead, how rapidly elevation changes within each square (van der Beek and Braun, 1998). This method has shown to be very useful to analyze the topographic signal produced by active tectonic structures and it is thought to be capable to identify areas with different uplift rates (Pérez-Peña et al., 2009b; Siddiqui and Soldati, 2014). We have selected a grid size of 1.5 km and used a DEM of 10 m of pixel resolution to derive HI values. This grid size is half the average mean-width of the analyzed basins (Table 1) in order to better characterize slope features at basin scale. We have used a DEM of 10 m of pixel resolution provided by the Junta de Andalucía regional government. This DEM was obtained by photogrammetry using 1:20,000 aerial photographs taken between 2001 and 2002. Once HI values were computed from the grid squares, we performed a hot-spot analysis by calculating the Getis-Ord spatial statistics with a threshold search distance of 20 km. This distance corresponds to the North–South width of the Sierra Nevada.

Table 1
Numerical values of morphometric indexes of the Sierra Nevada catchments.

Basin Id	Area (Km^2)	L (Km)	W (Km)	Ksn[a]	Fit θ	Ebulk[b]	|AF − 50|	Drainage
N01	34.47	11.22	3.07	29.45	0.24	9.74	18.34	North
N02	28.87	13.03	2.22	79.93	0.39	4.96	17.20	North
N03	53.08	17.21	3.08	121.49	0.54	12.03	12.01	North
N04	14.27	8.41	1.70	97.18	0.48	8.23	0.37	North
N05	23.55	11.03	2.14	188.36	0.48	9.84	24.47	North
N06	26.76	10.37	2.58	139.55	0.45	15.90	4.74	North
N07	17.83	9.44	1.89	143.40	0.45	10.35	6.32	North
N08	15.51	8.55	1.82	130.34	0.48	12.22	9.61	North
N09	14.51	8.12	1.79	94.10	0.31	10.07	1.13	North
N10	29.07	9.77	2.98	124.49	0.45	16.72	32.55	North
N11	17.74	9.34	1.90	105.83	0.41	11.71	3.65	North
N12	14.08	9.16	1.54	111.92	0.45	10.96	1.29	North
N13	33.64	11.48	2.93	112.98	0.44	13.78	3.05	North
N14	39.08	14.02	2.79	114.83	0.51	15.65	0.54	North
N15	60.00	15.53	3.86	119.84	0.42	15.39	4.28	North
N16	22.35	9.67	2.31	70.30	0.30	11.09	8.00	North
S01	32.99	17.18	1.92	184.69	−0.08	21.84	2.97	South (W)
S02	27.88	13.05	2.14	202.21	0.06	14.62	12.11	South (W)
S03	91.43	19.28	4.74	280.23	0.33	34.48	14.14	South (W)
S04	150.19	33.82	4.44	196.13	0.40	32.16	22.25	South (W)
S05	67.27	18.28	3.68	161.20	0.13	21.34	23.78	South (W)
S06	50.67	17.43	2.91	146.10	0.21	16.45	20.13	South (E)
S07	63.77	16.53	3.86	156.98	0.18	17.99	13.71	South (E)
S08	24.29	13.75	1.77	153.95	0.23	13.88	5.37	South (E)
S09	49.75	16.33	3.05	166.07	0.27	20.64	15.13	South (E)
S10	44.99	14.71	3.06	161.52	0.34	19.08	3.39	South (E)
S11	49.59	12.04	4.12	159.00	0.41	17.66	6.49	South (E)
S12	37.35	15.01	2.49	140.99	0.13	13.92	5.00	South (E)
S13	28.54	14.46	1.97	117.61	0.21	12.11	1.69	South (E)
W01	80.96	20.22	4.00	61.95	0.27	10.83	6.31	West
W02	140.04	26.16	5.35	96.87	0.17	18.38	10.53	West
W03	185.84	27.56	6.74	160.01	0.41	42.29	9.84	West
W04	57.78	20.59	2.81	174.22	0.34	20.00	2.11	West
W05	46.13	21.37	2.16	154.22	0.25	18.15	11.85	West
W06	47.13	17.82	2.64	175.04	0.24	18.59	10.87	South (W)
W07	22.94	9.81	2.34	204.71	0.38	15.09	8.64	South (W)

[a] θref: 0.45.
[b] 10^7 m^3/km^2.

3.1.3. Minimum bulk erosion (E_{bulk})

In order to determine long-term erosion at catchment scale, we have computed E_{bulk} (Menéndez et al., 2008; Giaconia et al., 2012; Azañón et al., 2012; Bellin et al., 2014). To do so, we have obtained a theoretical pre-incision surface for each catchment by interpolating elevations from present-day lateral divides. Bulk erosion is then calculated by computing the volume between this surface and present-day topography, which was normalized by catchment area. Minimum bulk erosion underestimates long-term erosion at basin scale, since it does not take into account interfluves lowering (Brocklehurst and Whipple, 2002; Pérez-Peña et al., 2010).

3.1.4. Asymmetry factor (AF)

The asymmetry factor (AF) of catchments was used to detect asymmetric catchments at the scale of the whole range (Keller and Pinter, 2002; Pérez-Peña et al., 2010). Asymmetric catchments can respond to tectonic tilting, lithologic fabric and/or capture processes. AF has been traditionally defined as:

$$AF = 100(Ar/At)$$

being Ar the area of the basin to the right (facing downstream) of the trunk channel and At the total area of the catchment. AF values greater

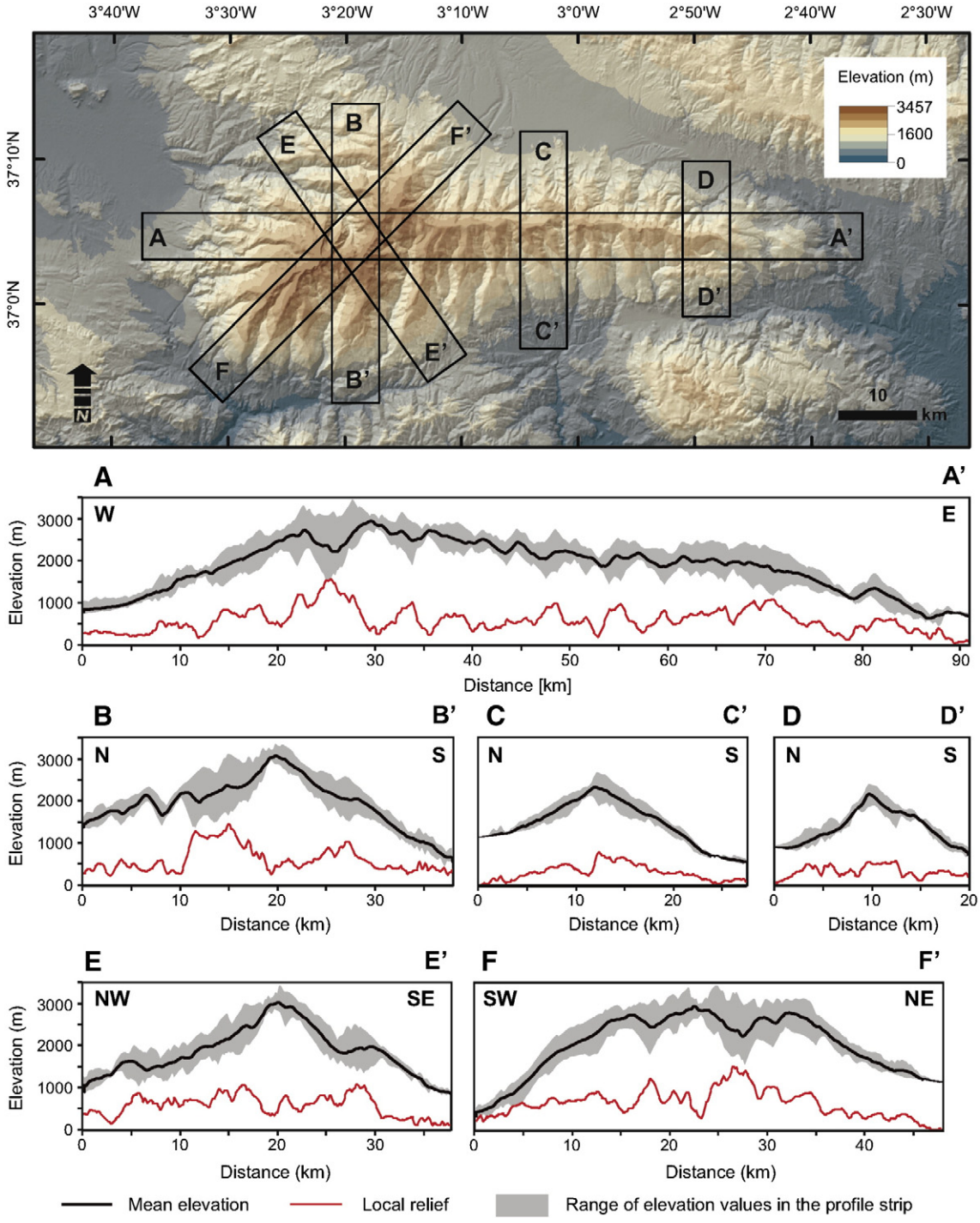

Fig. 2. DEM of the Sierra Nevada with location of the six swath profiles. Swath profiles showing the trend of the maximum, minimum, and mean topography of the Sierra Nevada. In each profile local relief has been computed by subtracting the minimum from the maximum elevation.

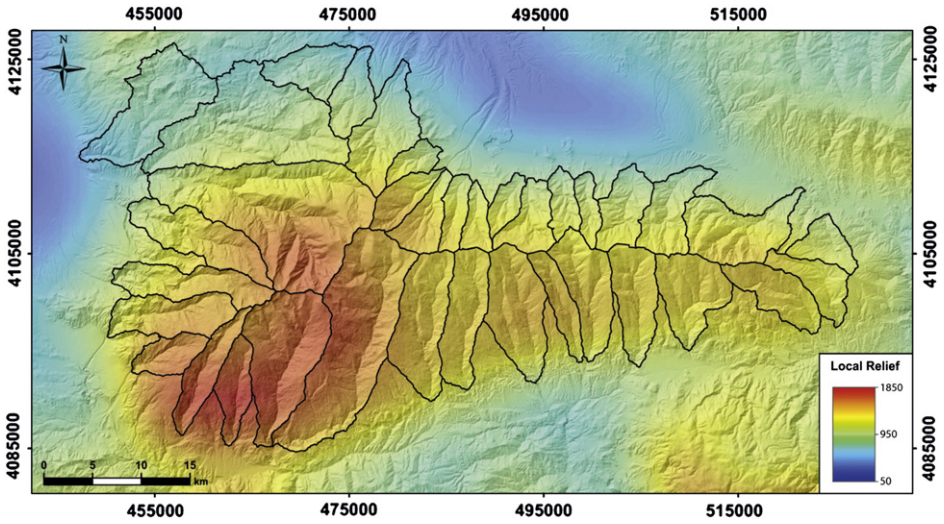

Fig. 3. DEM of the Sierra Nevada showing local relief calculation. The highest values are spatially correlated with the most elevated areas where the steepest gradients are observed.

or less than 50 may indicate tilt to the left or to the right respectively (Keller and Pinter, 2002). However, in order to avoid possible confusions between catchments located at the northern and southern slopes of the Sierra Nevada, we followed the methodology proposed by Pérez-Peña et al. (2010). We expressed the asymmetry as the absolute deviation of a perfect symmetric channel (AF = 50) together with an arrow indicating the asymmetry direction.

$$AF* = |50-(Ar/At)*100| + \text{orientation indicator (arrow)}$$

We have divided AF* values in four classes: AF < 5 (symmetric basins), AF = 5–10 (gently asymmetric basins), AF = 10–15 (moderately asymmetric basins), and AF > 15 (strongly asymmetric basins).

3.1.5. Normalised steepness index and concavity index

Graded rivers show an exponential relationship between channel slope (S) and up-stream area (A) (Hack, 1957). This well-known relation is described by the power-law:

$$S = k_s A^{-e}$$

where k_s is the channel steepness-index and Θ the concavity index (Flint, 1974). When slope and area data are represented in logarithmic-scale plots, this power relation yields a straight line that can be used to derive k_s and Θ by linear regression. This power-law relation has been used in several tectonic studies, since different area-slope relations can be due to active tectonics, changes in river bed lithology, and/or climate (Wobus et al., 2006; Kirby and Whipple, 2012; Whipple et al., 2013; Burbank and Anderson, 2013; Bellin et al., 2014; Scotti et al., 2014).

Some studies have proposed that the concavity index (Θ) varies in most natural channels in a narrow range between 0.4 and 0.6, being relatively insensitive to differences in uplift rate, lithology and/or climate at steady-state (Kirby and Whipple, 2012; Whipple et al., 2013). By contrast, the steepness index (ks) is highly sensitive to all the mentioned factors. In practice, the use of a normalized steepness index (k_{sn}) is preferred to avoid the strong correlation of k_s and Θ. The k_{sn} index is computed by considering a fixed concavity (Θ_{ref}) (Wobus et al., 2006; Kirby and Whipple, 2012; Whipple et al., 2013; Burbank and Anderson, 2013). Several studies have proposed a strong correlation between k_{sn} and uplift rate (e.g., Kirby and Whipple, 2012; Bellin et al., 2014).

We have derived the k_{sn} index for all the analyzed basins in the Sierra Nevada mountain range by regression of slope-area plots with the aid of open-source codes available from http://www.geomorphtools.org. We have used a Θ_{ref} of 0.45, as proposed in recent studies in the eastern Betics (Bellin et al., 2014) and NE Spain (Scotti et al., 2014).

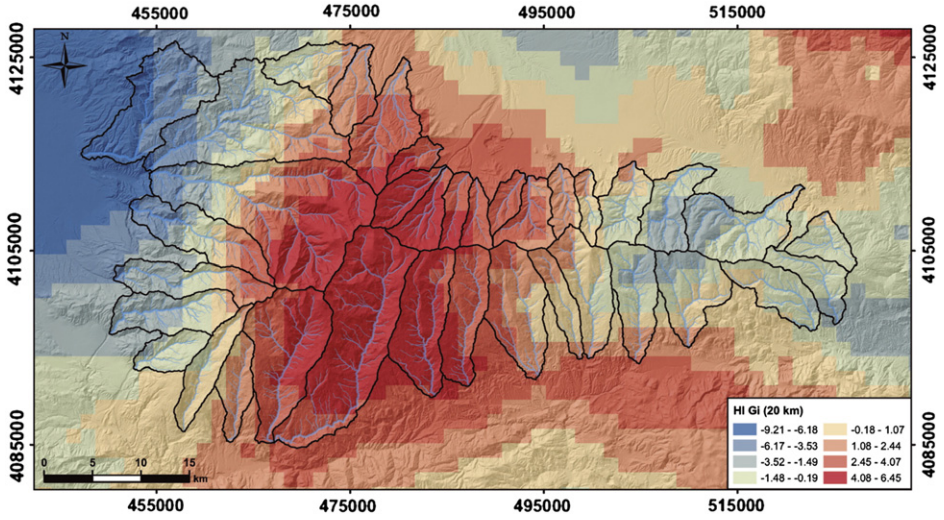

Fig. 4. Hypsometrical integral estimates on DEM of Sierra Nevada. HI has been calculated by pixels of 2.25 km^2 (see explanation on the text). The zones potentially influenced by tectonics are distinguished by the highest values.

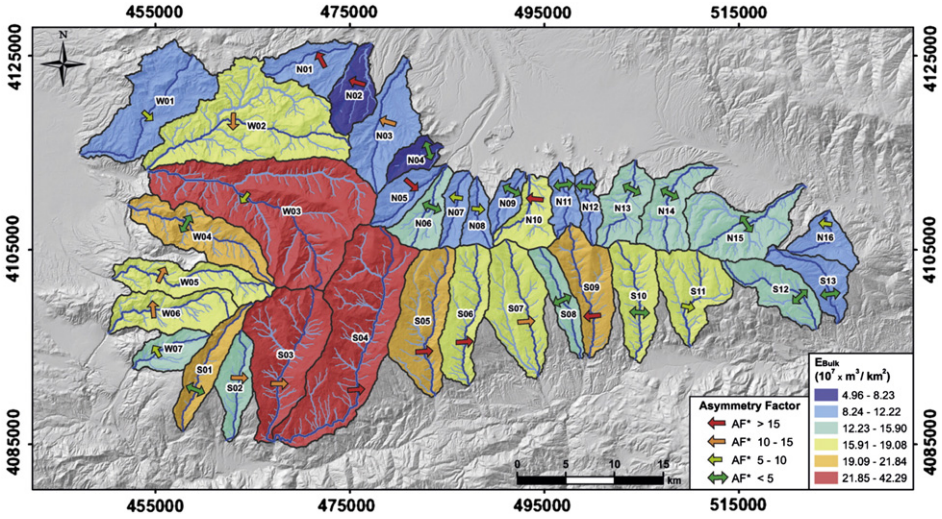

Fig. 5. Minimum bulk erosion (E_{bulk}) estimates on river catchments of Sierra Nevada. Asymmetry Factor (AF*) values in all the river catchments of Sierra Nevada. AF* has been calculated as the absolute deviation of a perfect symmetric channel with AF = 50 (see explanation in the text).

3.2. Drainage network analysis

The general drainage pattern of the Sierra Nevada has been analyzed through the study of preferential orientations. To perform the drainage orientation analysis, we have divided the Sierra Nevada in four parts attending the main topographic features: "Sierra W" includes the western termination with the highest elevations, "Sierra E" represents the eastern termination and the lowest elevations of the mountain range, "Sierra Central" represents the central part with intermediate elevation, and "Sierra NW" includes the northwesternmost termination where the boundary of the mountain range is more diffuse and lower elevation and gentler gradients dominate.

The drainage network analysis has not been yet carried out in Sierra Nevada and the conventional technique has been improved adding a novel calculation. Firstly, the drainage network has been generalized by simplifying the flow lines with a specified maximum offset tolerance, thus removing the sinuosity of the channels. This operation transforms the undulating drainage network into rectilinear segments that represent the dominant orientations. Then, the resulted segments have been divided in equal length stretches of 50 m. The orientation of each segment has been calculated and rose diagram plots have been produced.

We have carried out a supplementary calculation in addition to the conventional methodology. We have verified if the simplified (rectilinear) flow lines follow the theoretical steepest direction through the mountain range. This has been defined as "the orientation parallel to the slope aspect of a simplified model of the relief". That simplified model may be a filtered topography model or a relief envelope. If the direction of a channel segment is offset from the direction of the slope aspect of the simplified topography by a specified azimuth angle, this segment is considered "anomalous". These anomalous segments may reveal orientations related to wind gaps or rivers conditioned by lithological contacts or tectonic structures that affect the rock massif. The described method acts as a filter of information that helps in the interpretation of lineaments associated to the drainage network. The method is based implicitly on the following assumption: the erosion follows the steepest slope as analogue and numerical (see e.g., Babault et al., 2012) models indicate. The main drawback of the method is that it does not detect anomalous orientations parallel to the slope aspect. Thus, anomalous and non-anomalous channels have been represented

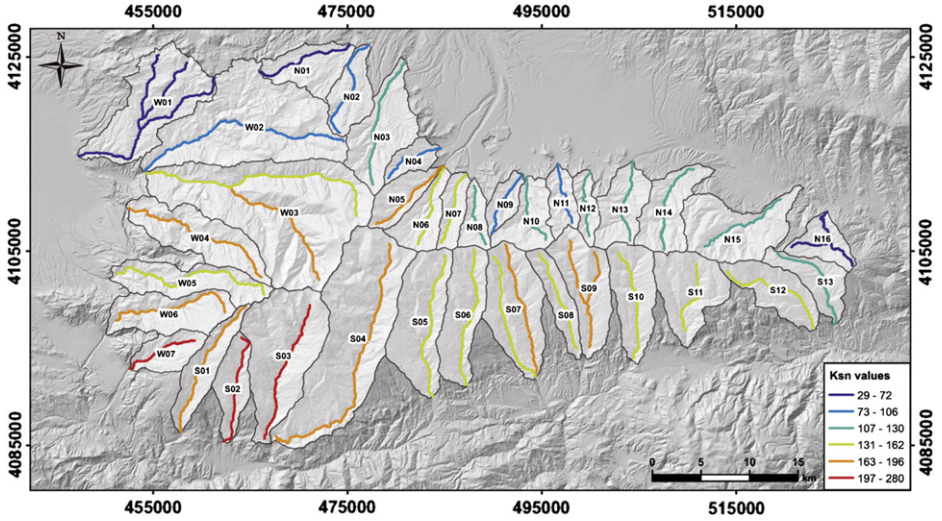

Fig. 6. Map of channel normalized steepness indices (k_{sn}) extracted throughout the Sierra Nevada. To derive k_{sn} values we used a Θ_{ref} of 0.45, as proposed in recent studies in the eastern Betics (Bellin et al., 2014) and NE Spain (Scotti et al., 2014).

together in the rose diagrams to identify preferential orientations not defined as anomalous but possibly related to structural elements or lithological contacts.

In order to evaluate possible anomalous channels in the Sierra Nevada, we have derived the regional slope of this mountain range by using the same relief envelope as in the case of the local relief (see Section 3.1). This envelope connects maximum topographic elevations with a smoothed surface that removes the roughness and curvature produced by river incision. Channels with azimuths that deviate from regional slope orientation more than 45° are considered as channels with anomalous orientation.

3.3. Denudation rates and uplift pattern mapping

In order to obtain numerical denudation rates, we use the compilation by Kirby and Whipple (2012), where these authors plot the relationships

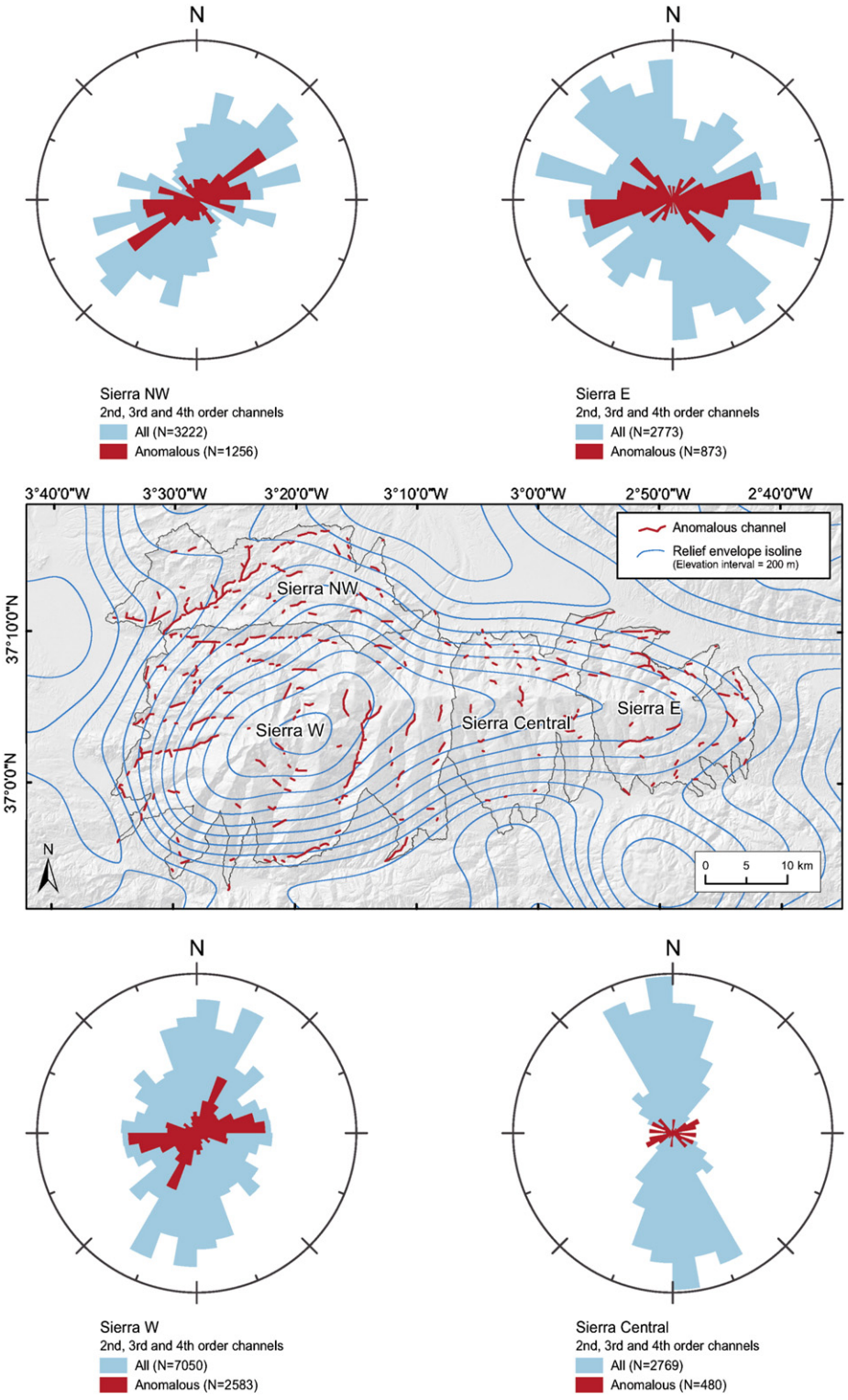

Fig. 7. Relief envelope isoline map showing anomalous channel orientation (>45°) respect to expected stream azimuths assuming as normal flow in the main regional slope direction. The change from an E–W to NE–SW main divide between the central and western Sierra Nevada is related to the active NE–SW oriented antiform.

between normalized channel steepness values and denudation rates, extracted from ^{10}Be estimations, for a variety of active orogens. Denudation rates obtained in this way were compared with long term uplift rates (Braga et al., 2003). We have applied the Universal Kriging method for mapping the spatial pattern of these uplift rates. This method interpolates spot values of a dependent variable on the basis of auxiliary variables. In our case, the dependent variable is the uplift rate and the auxiliary variable is the elevation. Thus, the elevation can be used to predict uplift rates in areas without information, because both parameters directly correlate. On the other hand, the outcrops studied by Braga et al. (2003) have been used to make a spatial interpolation in the landscape and the DEM. The solution applied to this problem was to use a relief envelope as the auxiliary variable to adjust reasonably well to uplift values. The prediction model of these uplift rates in raster format was generated by SAGA (System for Automated Geoscientific Analyses). The isolines map that represents an estimate of the mean uplift rates in the study area has been derived from that model.

4. Geomorphic autopsy of the Sierra Nevada based on topographic metrics and drainage network analysis

4.1. Relief analysis

Regarding the swath profiles, the Sierra Nevada E–W longitudinal profile shows that the highest elevations and local relief values are reached in the W sector (A–A′ in Fig. 2). The altitude values along the profile allow differentiating two sectors: the elevation in the western high mountain area is mainly concentrated between 2000 and 3000 m, whereas altitude values of the headwaters in the E sector fall in the range 1500–2500 m. On the other hand, the westernmost side shows a straight slope leading into the Granada basin (local base-level at about 650 m), while the easternmost slope exhibits a convex hillside that connects to the Nacimiento River (with a base-level in the Mediterranean Sea). N–S and oblique profiles (B–B′, C–C′, D–D′, E–E′ and F–F′ in Fig. 2) show straight to concave slopes in the N slope leading into the Guadix basin (a local base-level at about 1000 m) and convex hillsides in the S slope (connected to the rivers that flow into the Mediterranean Sea). Local relief and hypsometric analysis in the Sierra Nevada bring similar results, which are also compatible with erosion bulk and k_{sn} data. The highest values of local relief (Fig. 3) are in the southwestern part of the Sierra Nevada, in accordance with the area of maximum altitudes. Mediterranean draining catchments at the central and eastern parts of the Sierra Nevada present intermediate values. The lowest values are associated to the Atlantic draining catchments located at the northern slope of the Sierra Nevada where there is a local base-level of around 1000 m.

In the same way, the hypsometric analysis yields a clear cluster located in the western part of the Sierra Nevada, including a wide area of approximately 30 km North–South and 20 km East–West (Fig. 4). The center of this cluster coincides with the highest elevations. Apart of this main cluster, the northern and southern borders of the Sierra also present different HI patterns. The southern slope (Mediterranean catchments) matches with high values, whereas such pattern is not observed at the northern slope (Atlantic catchments).

The general pattern of minimum erosion bulk values in the Sierra Nevada (Fig. 5) is also similar to local relief and HI results. The lowest values are associated with the Atlantic catchments draining to the Guadix basin, whereas the highest values concentrate in the western part coinciding with the highest elevations of the mountain range. In this sector, there are three catchments (W03, S03 and S04 in Fig. 5) with extremely high values of this parameter, which could be related to a high rate of erosion on the fold hinge area of a NE–SW oriented active fold (Azañón et al., 2012). Intermediate values of minimum erosion bulks appear in the Mediterranean catchments of the southern Sierra Nevada and in the Atlantic catchments draining to the Granada Basin.

AF values in the western Sierra Nevada present a pattern with opposite asymmetries at both sides to the Lanjarón River (Pérez-Peña et al., 2010; Azañón et al., 2012), thus coinciding with the fold hinge of a NE–SW oriented antiform (Table 1, Fig. 5). In the eastern Sierra Nevada, AF values do not show a defined pattern, with the majority of the basins being symmetric (AF < 5).

The highest values of K_{sn} are located at the western part of the mountain range. Furthermore, northern (Atlantic) catchments have generally lower values of k_{sn} than southern (Mediterranean) ones (Fig. 6). The lowest values of k_{sn} are located at the easternmost end of the Sierra Nevada and along two catchments of the northern mountain front (W01, N01); these values are comparable to those calculated for the eastern Betics by Bellin et al. (2014).

4.2. Drainage network analysis

The eastern Sierra Nevada streams present a clear E–W trend in anomalous channel orientation (Fig. 7). These transverse anomalous channels run parallel to E–W striking compressional structures. Gentler regional slope in this part of the mountain range could be counteracted by structure-controlled local slopes, as has been proposed for streams of

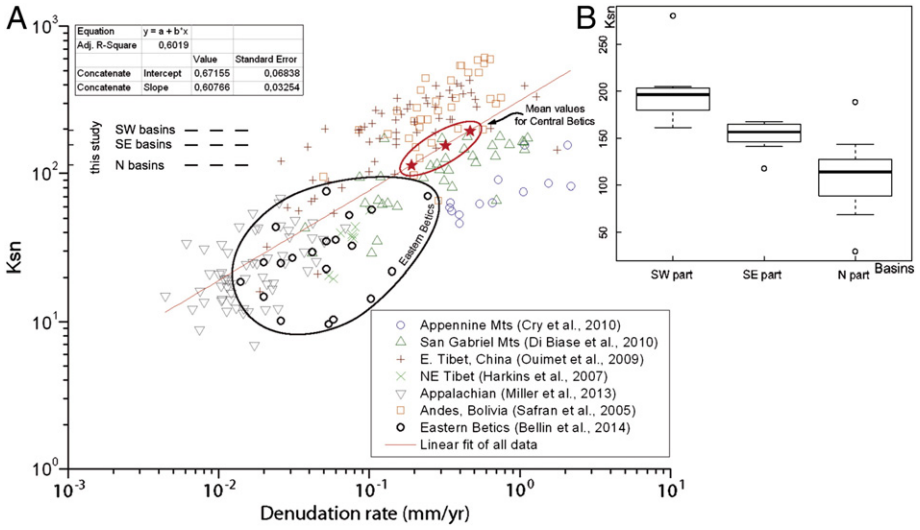

Fig. 8. A) Empirical scaling relationships between normalized steepness channels (k_{sn}) and denudation rates from a variety of active orogens (figure adapted from Kirby and Whipple (2012). Data from Eastern Betics have been extracted from Bellin et al. (2014). B) Mean values of k_{sn} for Sierra Nevada.

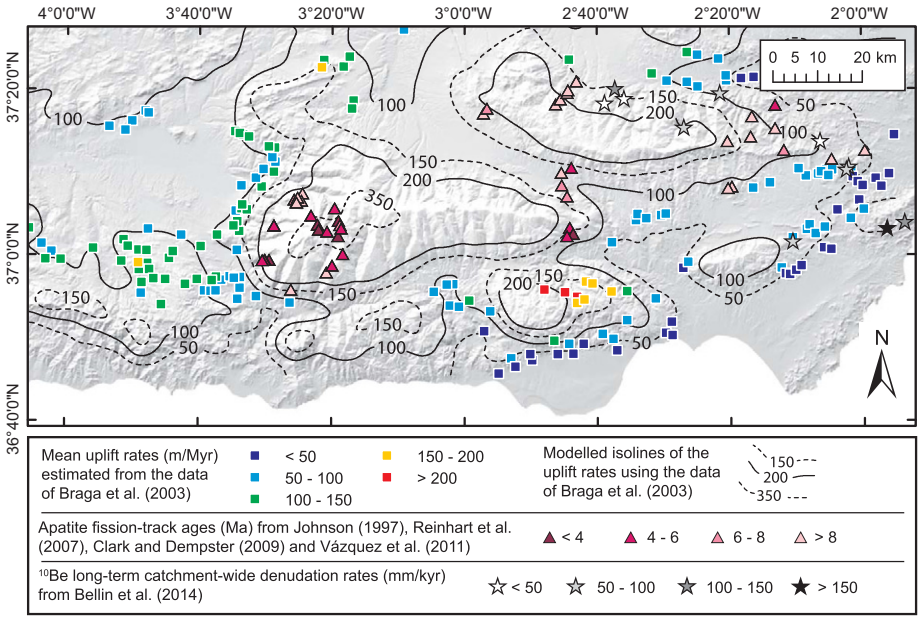

Fig. 9. Modeled isolines for uplift rates using the data from Braga et al. (2003) (see text for explanation). Apatite fission-track ages (Ma) are derived from Johnson (1997), Reinhardt et al. (2007), Clark and Dempster (2009) and Vázquez et al. (2011). ^{10}Be long-term catchment-wide denudation rates (mm/year) are taken from Bellin et al. (2014).

the Atlas by Babault et al. (2012). In the central Sierra Nevada there are also E–W directed anomalous channels, but they are considerably less frequent, probably due to the steeper regional slope in this sector. The western Sierra Nevada presents two anomalies oriented NNE–SSW and E–W. These anomalous channels are transverse to the NE–SW active fold, probably representing a progressive river network adaptation to the new regional slope promoted by this active structure (Azañón et al., 2012). Finally, NE–SW oriented anomalies in the NW Sierra Nevada could respond to structure-controlled segments related to an active NE–SW oriented synform.

Uplift pattern mapping, which is derived from the location of Tortonian coastal deposits, shows highest mean values for the western

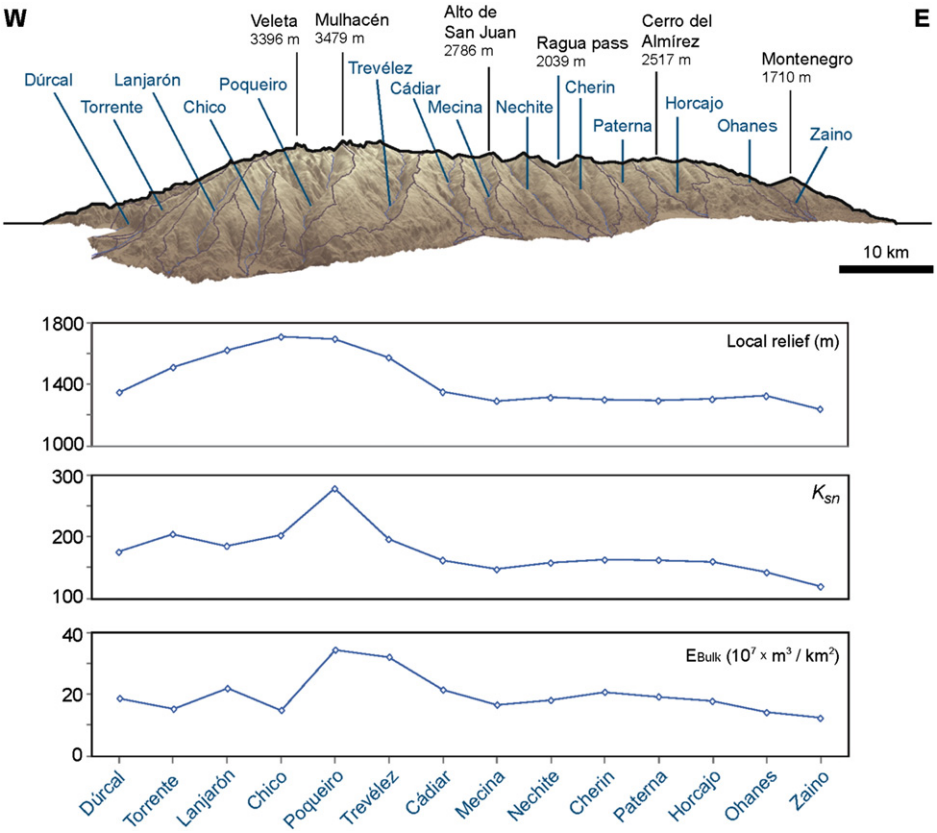

Fig. 10. Local relief, Normalized steepness channels and minimum bulk erosion values along the southern catchments of Sierra Nevada. This plot represents the changes of the mentioned indexes along the basins of the South margin of the Sierra, i.e., in equal hydrological and geological setting. Thus, the observed variation should be related to tectonic activity because the other parameters that may condition the values of the indexes are roughly similar throughout this margin of the Sierra.

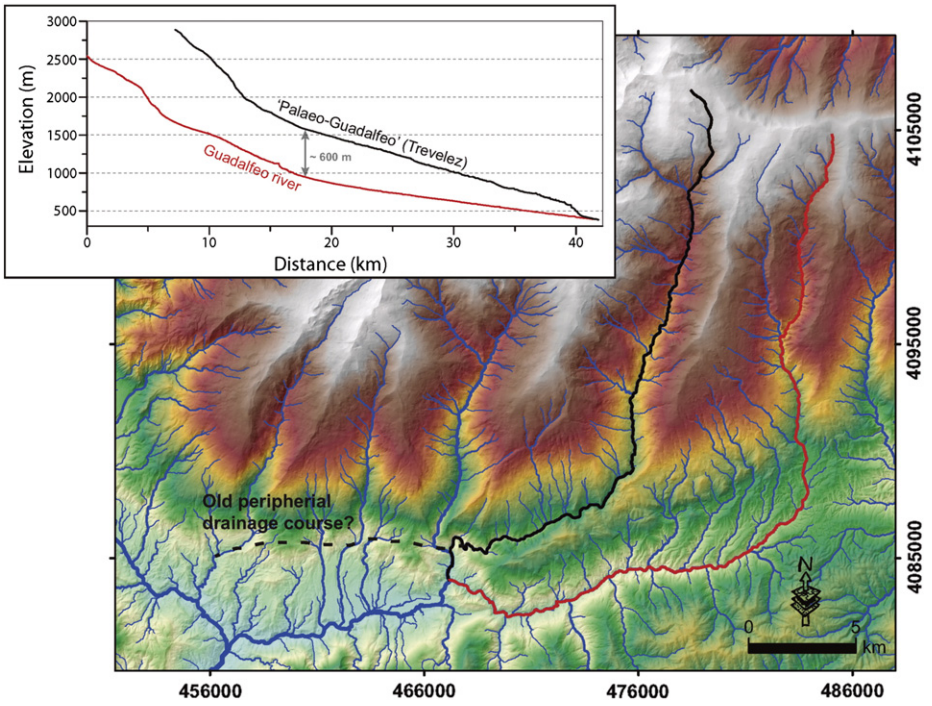

Fig. 11. DEM of the western sector of Sierra Nevada showing the southern (Trevelez) E–W rivers as a water-gap raised 600 m from the current position of the Guadalfeo river (local base level).

sector of the Sierra Nevada. Mean values in this sector are between 0.4 and 0.5 mm/year, whereas values from the eastern sector are between 0.15 and 0.2 mm/year (Fig. 8). Values for the easternmost sector of the Betic Cordillera obtained by ^{10}Be are between 0.015 and 0.15 mm/year (Bellin et al., 2014). The isolines map shows that the highest average uplift rates (>0.35 mm/year) concentrate in the same sector, where the most recent AFT ages have been obtained (references included in Fig. 9).

5. Discussion

Since river erosion is driven by the constant competition between uplift and climate (Burbank, 1992), the variation of relief incision in an area with almost constant climate indicates the rivers' response to different tectonic inputs. However, local circumstances, such as lithological changes, structural and mechanical discontinuities and the presence of local base-levels are proxies that should be considered in

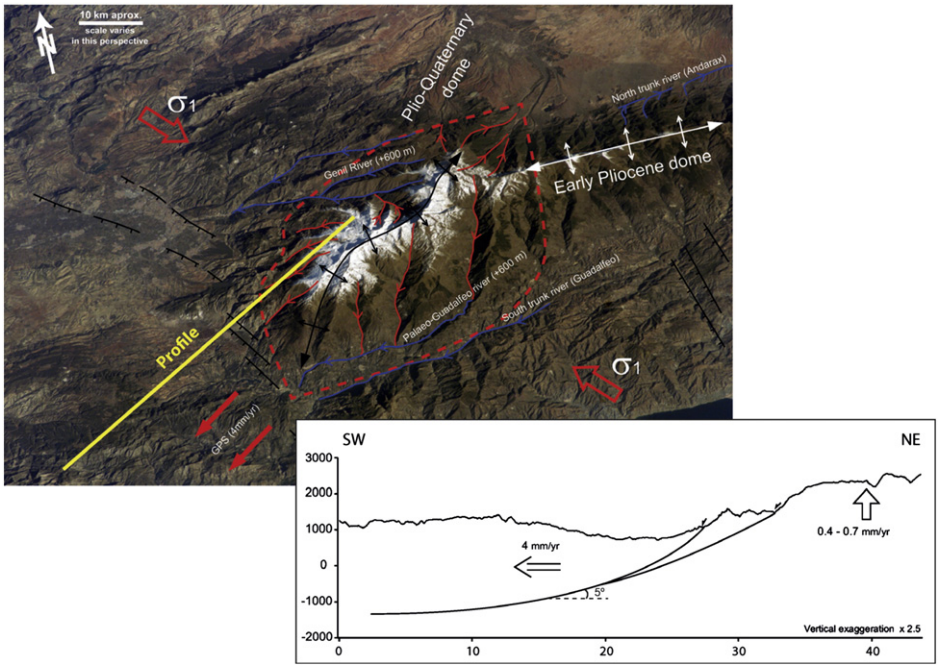

Fig. 12. Cartoon of the western sector of Sierra Nevada showing the relationships between the Plio-Quaternary NE–SW fold, NW–SE westward extensional faults, σ1 regional stress and the drainage pattern.

order to evaluate the role of tectonics. In terms of lithology, the Sierra Nevada has a relative homogeneity because it is mostly formed by graphite schists and quartzites from the Nevado–Filabride Complex. However, regional scale structures and local base-levels could explain some of the variations in the evolution of the drainage pattern and the denudation parameters. Thus, the northern and southern mountain fronts of the Sierra Nevada (excluding the western termination) are very different from structural and geomorphic points of view. The northern mountain front corresponds with a discordance between the Guadix basin sediments and the Nevado–Filabride metamorphic basement, whereas the southern border one is structurally controlled by E–W strike-slip transfer faults (Martínez-Martínez et al., 2006; Pérez-Peña et al., 2010) that link to NW–SE westward-directed normal faults outcropping in the western border. The geomorphic characteristics of rivers north and south of the Sierra Nevada are also quite different; the northern rivers local base level is located at ~1000 m Guadix basin (with an endorheic character until the Late Pleistocene; Azañón et al., 2005; Azañón et al., 2006; García-Tortosa et al., 2008; Pérez-Peña et al., 2009c; Fernández-Ibañez et al., 2010) and drainage flows to the Atlantic through the Guadalquivir River, whereas in southern rivers local base-level is located at ~500 m and drainage is finally directed to the Mediterranean Sea, located less than 25 km south of the Sierra Nevada southern mountain front. Local base level at the western border is also controlled by NW–SE oriented active normal faults that individualize Sierra Nevada from the Granada basin (~600 masl). This basin has also been endorheic until Early Pleistocene (e.g., Azañón et al., 2004; García-Alix et al., 2009).

These differences in the local base-level between the northern, southern and western slopes of the Sierra Nevada are controlling the results of topographic metrics. Thus, northern catchments draining to the Guadix basin show the lowest values of bulk erosion and steepness parameters. Moreover, bedrock river profiles draining to the north show significant differences of concavity with respect to rivers draining to the south (B–B′, C–C′ and D–D′ in Fig. 2). Northern bedrock river profiles have the typical geometry of highly eroded catchments with a high concavity, whereas the southern ones have a convex geometry, which is usually associated with rejuvenated topography.

The variations in local base-level around the Sierra Nevada have been previously explained by the contrast in the tectonic activity between its borders (Pérez-Peña et al., 2010). The western and southern edges host active faults, whereas the northern border is an unconformity that probably underwent the most recent part of the uplift history of Sierra Nevada. Therefore, contrasting results observed in the concavity, steepness and bulk erosion values between northern and southern slopes appear to be chiefly controlled by local base-levels, which are directly related to the most recent tectonic history of Sierra Nevada.

5.1. Differential tectonic activity along the Sierra Nevada

All the morphometric parameters extracted from topography and streams show highest values in the western Sierra Nevada (Figs. 4 to 7). To avoid the influence of local base levels in the variations between the western, central and eastern Sierra Nevada, we have decided to restrict our analysis to southern catchments, which have also a uniform lithology and climate characteristics. In Fig. 10, we compare local relief, K_{sn} and E_{bulk} erosion in those basins. The highest values of the three parameters are concentrated between the Lanjarón and Cádiar river catchments in the western Sierra Nevada, where HI index also indicates the highest anomaly. Thus, we conclude that the highest denudation indicators are measured in the western Sierra Nevada coinciding with the hinge area of the NE–SW oriented active antiform. AFT data are also consistent with the presence of this NE–SW fold (Fig. 5), which would be younger than the E–W oriented Pliocene open fold.

The western Sierra Nevada concentrates most part of the anomalous streams (Fig. 7). We interpreted all these alterations of the drainage pattern linked to: (1) water gaps inherited from the recent elevation of the longitudinal drainage belonging to the outer areas of the E–W oriented Sierra Nevada antiformal ridge; and (2) structural features that control the drainage network (i.e., folds, faults or tensional joints). In this sense, the change from an E–W to NE–SW main divide between the central and western Sierra Nevada is related to the active NE–SW oriented antiform.

Coming back to the first hypothesis on western anomalous streams, we consider northern and southern main rivers of the western Sierra Nevada as trunk axial rivers of an E–W range that have been raised in a younger uplift phase. This is the case of the Genil river in the north and the so-called palaeo-Guadalfeo (lower part of the Trevélez river) in the south (Fig. 11). Both rivers have an anomalous E–W orientation, parallel to the main axis of the Sierra Nevada dome. The Genil river has a mean elevation 600 m higher than the Andarax river, which is the current axial trunk river of the northeastern termination of the Sierra Nevada dome. In the southern flank of Sierra Nevada, the so-called palaeo-Guadalfeo river has a differential elevation respect to current Guadalfeo River that ranges between 600 and 1000 m (Fig. 11).

5.2. Uplift and folding of the westernmost Sierra Nevada related to orthogonal westward extensional detachments

Our results indicate that the western sector of the Sierra Nevada concentrate the most recent tectonic activity. Thus, a NE–SW active open fold, which is sub-perpendicular to the current σ1 regional stress, is causing stream deflections and wind gaps on the old longitudinal drainage pattern (Fig. 12). This fold also controls the position of the main divide of the western ending of Sierra Nevada. This active structure is also compatible with extensional listric faults that constitute the edge between Sierra Nevada and the Granada basin (Fig. 12).

Current GPS movements (Mancilla et al., 2013) in the Granada basin (3–4 mm/year in WSW-ward direction) contrast with no relative movements of the Sierra Nevada in this direction (Fig. 12). Consequently, we can hypothesize that listric normal faults of the western edge of Sierra Nevada are producing this displacement. As can be seen in the cross-section of Fig. 12, derived from the interpretation of reflection seismic profiles, these faults have a listric geometry rooting in a flat extensional detachment (e.g., Rodríguez-Fernández and Sanz de Galdeano, 2006; Rodríguez-Fernández et al., 2012). Therefore, a mean dip between 5–10° can be a realistic value for these faults. In this case, a relative uplift of 0.4–0.7 mm/year for the footwall will be concordant with a westward movement of 3–4 mm/year for the hanging wall.

6. Conclusions

a) River incision in Sierra Nevada is mainly conditioned by tectonics and local or regional base level. Northern bedrock river profiles have a high index of concavity whereas the southern ones have a convex geometry, which is commonly associated to rejuvenated topography. Normalized steepness channels index and minimum bulk erosion also indicate a sharp contrast between northern and southern river catchments of Sierra Nevada, presenting the northern ones the lowest values of these parameters. Active tectonics in the southern and western borders of Sierra Nevada and, mainly, the presence of Guadix basin (northern sector) ~400–500 m higher than Granada basin (western sector) or Guadalfeo river (southern sector) induce different river profile evolutionary histories. This geomorphic analysis provides a very consistent general framework of relief erosion and river incision controlled by local base levels. However, once this factor has been discounted, outstanding differences regarding recent tectonic activity between the western and eastern Sierra Nevada emerge.

b) The western sector of Sierra Nevada, where main elevations are concentrated, presents the highest values of all topography depending parameters (Local relief, k_{sn}, Erosion volume, HI). Normalized steepness channel values in this sector, which have empirically

been correlated with denudation rates (Kirby and Whipple, 2012), show a remarkable difference from the Eastern Betics (Bellin et al., 2014). Concerning the southern river catchments of Sierra Nevada, where lithology, climatology and base-level are uniform, the gradual eastward decrease of the denudation rates has been observed. On the other hand, mean values of uplift, collected from current elevation of coastal deposits from Late Tortonian (Braga et al., 2003), of the western sector are comprised between 0.3–0.4 mm/year whereas in the eastern sector are comprised between 0.1–0.2 mm/year. Active folding, sub-perpendicular to the current maximum regional shortening, and compatible westward extensional faulting could be the cause of this anomalous uplift and denudation rates of the western sector.

c) The recent uplift of the western sector in Sierra Nevada transforms old longitudinal drainage of this area in water gaps (Genil river to the north and the so-called "paleo-Guadalfeo" to the south that are hanging around 600 m above their original altitudes) or produced deflections in the drainage pattern linked to a NE–SW active folding.

d) Our quantitative results show that denudation rate values in Sierra Nevada are consistent with mean uplift values that have been obtained by an independent method. Consequently, we can conclude that there is a steady-state between uplift and denudation in the Central Betic Cordillera.

e) GPS results (Mancilla et al., 2013) agree with faulting style and orientation inferred from moment tensor inversion. While compression along the convergent limit aligns with Nubia–Eurasia relative plate motion, extension in the central Betics cannot be understood in terms of plate convergence and thin-shell tectonics, confirming that sub-crustal geodynamics operate here.

Acknowledgments

This study was supported by research projects CGL-2011-29920, TOPOIBERIA CONSOLIDER-INGENIO 2010 from the Spanish Ministry of Science and Innovation and the RNM-148 Research Group from the Junta de Andalucía. Spanish "Juan de la Cierva" grants support one of the researchers of this study. Authors also wish to acknowledge the review of two anonymous reviewers and guest-editor Javier A. Pulgar.

References

Alfaro, P., Galindo-Zaldívar, J., Jabaloy, A., López-Garrido, A.C., Sanz de Galdeano, C., 2001. Evidence for the activity and paleoseismicity of the Padul fault (Betic Cordillera, southern Spain). Acta Geol. Hisp. 36, 283–295.

Azañón, J.M., Azor, A., Booth-Rea, G., Torcal, F., 2004. Small-scale faulting, topographic steps and seismic ruptures in the Alhambra (Granada, southeast Spain). J. Quat. Sci. 19, 219–227.

Azañón, J.M., Azor, A., Pérez-Peña, J.V., Carrillo, J.M., 2005. Late Quaternary large-scale rotational slides induced by river incision: the Arroyo de Gor area (Guadix basin, SE Spain). Geomorphology 69, 152–168.

Azañón, J.M., Tuccimei, P., Azor, A., Sánchez-Almazo, I.M., Alonso-Zarza, A.M., Soligo, M., Pérez-Peña, J.V., 2006. Calcrete features and age estimates from U/Th dating: implications for the analysis of Quaternary erosion rates in the northern limb of the Sierra Nevada range (Betic Cordillera, southeast Spain. In: Alonso-Zarza, A.M., Tanner, L.H. (Eds.), Paleoenvironmental record and applications of calcretes and palustrine Carbonates. Geology Society of America Special Paper 416, pp. 223–239 (Boulder, Colorado).

Azañón, J.M., Pérez-Peña, J.V., Giaconia, F., Booth-Rea, G., Martínez-Martínez, J.M., Rodríguez-Peces, M.J., 2012. Active tectonics in the central and eastern Betic Cordillera through morphotectonic analysis: the case of Sierra Nevada and Sierra Alhamilla. J. Iber. Geol. 38, 225–238.

Azor, A., Keller, E.A., Yeats, R.S., 2002. Geomorphic indicators of active fold growth: South Mountain–Oak Ridge anticline, Ventura basin, southern California. Geol. Soc. Am. Bull. 114, 745–753.

Babault, J., Van Den Driessche, J., Teixell, A., 2012. Longitudinal to transverse drainage network evolution in the High Atlas (Morocco): the role of tectonics. Tectonics 31, TC4020.

Balanyá, J.C., García-Dueñas, V., 1987. Les directions structurales dans le Domaine d'Alborán de part et d'autre du Détroit de Gibraltar. C. R. Acad. Sci. 304, 929–932.

Behr, W.M., Platt, J.P., 2012. Kinematic and thermal evolution during two-stage exhumation of a Mediterranean subduction complex. Tectonics 31, TC4025.

Bellin, N., Vanacker, V., Kubik, P.W., 2014. Denudation rates and tectonic geomorphology of the Spanish Betic Cordillera. Earth Planet. Sci. Lett. 390, 19–30.

Booth-Rea, G., Azañón, J.M., García-Dueñas, V., Augier, R., 2003. Uppermost Tortonian to Quaternary depocentre migration related with segmentation of the strike-slip Palomares Fault Zone, Vera Basin (SE Spain). Compt. Rendus Geosci. 335, 751–761.

Booth-Rea, G., Azañón, J.M., García-Dueñas, V., 2004. Extensional tectonics in the northeastern Bethics (SE Spain): case study of extension in a multilayered upper crust with contrasting rheologies. J. Struct. Geol. 26, 2039–2058.

Booth-Rea, G., Azañón, J.M., Martínez-Martínez, J.M., Vidal, O., García-Dueñas, V., 2005. Contrasting structural and P–T evolution of tectonic units in the southeastern Betics: key for understanding the exhumation of the Alboran Domain HP/LT crustal rocks (western Mediterranean). Tectonics 24, TC2009.

Braga, J.C., Martín, J.M., Quesada, C., 2003. Patterns and average rates of late Neogene–recent uplift of the Betic Cordillera, SE Spain. Geomorphology 50, 3–26.

Brocklehurst, S.H., Whipple, K.X., 2002. Glacial erosion and relief production in the Eastern Sierra Nevada, California. Geomorphology 42, 1–24.

Burbank, D.W., 1992. Causes of recent Himalayan uplift deduced from deposited patterns in the Ganges basin. Nature 357, 680–683.

Burbank, D.W., Anderson, R.S., 2013. Tectonic Geomorphology. second ed. Blackwell Science, Oxford.

Burbank, D.W., Leland, J., Fielding, E., Anderson, R.S., Brozovic, N., Reid, M.R., Duncan, C., 1996. Bedrock incision, rock uplift and threshold hillslopes in the northwestern Himalayas. Nature 379, 505–510.

Calvache, M.L., Viseras, C., 1997. Long-term control mechanisms of stream piracy processes in southeast Spain. Earth Surf. Process. Landf. 22, 93–105.

Clark, S.J.P., Dempster, T.J., 2009. The record of tectonic denudation and erosion in an emerging orogen: an apatite fission-track study of the Sierra Nevada, southern Spain. J. Geol. Soc. 166, 87–100.

Comas, M.C., Platt, J.P., Soto, J.I., Watts, A.B., 1999. The origin and tectonic history of the Alboran Basin: insights from Leg 161 results. Proceedings of the Ocean Drilling Program: Scientific Results, pp. 555–580.

Cyr, A.J., Granger, D.E., 2008. Dynamic equilibrium among erosion, river incision, and coastal uplift in the northern and central Apennines, Italy. Geology 36, 103–106.

Dadson, S.J., Hovius, N., Chen, H., Dade, W.B., Hsieh, M.-L., Willett, S.D., Hu, J.-C., Horng, M.-J., Chen, M.-C., Stark, C.P., Lague, D., Lin, J.-C., 2003. Links between erosion, runoff variability and seismicity in the Taiwan orogen. Nature 426, 648–651.

Demets, C., Gordon, R.G., Argus, D.F., Stein, S., 1990. Current plate motions. Geophys. J. Int. 101, 425–478.

Demets, C., Gordon, R.G., Argus, D.F., Stein, S., 1994. Effect of recent revisions to the geomagnetic reversal time scale on estimates of current plate motions. Geophys. Res. Lett. 21, 2191–2194.

DeMets, C., Gordon, R.G., Argus, D.F., 2010. Geologically current plate motions. Geophys. J. Int. 181, 1–80.

Densmore, A.L., Gupta, S., Allen, P.A., Dawers, N.H., 2007. Transient landscapes at fault tips. J. Geophys. Res. 112, F03S08. http://dx.doi.org/10.1029/2006JF000560.

Dethier, D.P., Ouimet, P.R., Bierman, D.H., Rob, D.H., Balco, G., 2014. Basins and bedrock: spatial variation in ^{10}Be erosion rates and increasing relief in the southern Rocky Mountains, USA. Geology 42, 167–170.

Dumont, J.F., Santana, E., Vilema, W., 2005. Morphologic evidence of active motion of the Zambapala Fault, Gulf of Guayaquil (Ecuador). Geomorphology 65, 223–239.

Fernández-Ibañez, F., Pérez-Peña, J.V., Azor, A., Soto, J.I., Azañón, J.M., 2010. Normal faulting driven by denudational isostatic rebound. Geology 38, 643–646.

Flint, J.J., 1974. Stream gradient as a function of order, magnitude, and discharge. Water Resour. Res. 10, 969–973.

Galindo-Zaldívar, J., Gonzalez-Lodeiro, F., Jabaloy, A., 1989. Progressive extensional shear structures in a detachment contact in the western Sierra Nevada, (Betic Cordilleras, Spain). Geodin. Acta 3, 73–85.

Galindo-Zaldívar, J., Gil, A.J., Borque, M.J., González-Lodeiro, F., Jabaloy, A., Marín-Lechado, C., Ruano, P., Sanz de Galdeano, C., 2003. Active faulting in the internal zones of the central Betic Cordilleras (SE, Spain). J. Geodyn. 36, 239–250.

García-Alix, A., Minwer-Barakat, R., Martin, J.M., Martin-Suarez, E., Freudenthal, M., 2009. Dating the change from endorheic to exorheic conditions in the drainage system of the Granada basin (Southern Spain). Palaios 24, 544–549.

García-Dueñas, V., Balanyá, J.C., Martínez-Martínez, J.M., 1992. Miocene extensional detachments in the outcropping basement of the northern Alboran Basin (Betics) and their tectonic implications. Geo-Mar. Lett. 12, 88–95.

García-Tortosa, F.J., Alfaro, P., Galindo-Zaldívar, J., Gibert, L., López-Garrido, A.C., Sanz de Galdeano, C., Ureña, M., 2008. Geomorphologic evidence of the active Baza Fault (Betic Cordillera, South Spain). Geomorphology 97, 374–391.

Giaconia, F., Booth-Rea, G., Martínez-Martínez, J.M., Azañón, J.M., Pérez-Peña, J.V., Pérez-Romero, J., Villegas, I., 2012. Geomorphic evidence of active tectonics in the Sierra Alhamilla (eastern Betics, SE Spain). Geomorphology 145–146, 90–106.

Gómez-Pugnaire, M.T., Rubatto, D., Fernández-Soler, J.M., Jabaloy, A., López-Sánchez-Vizcaíno, V., González-Lodeiro, F., Galindo-Zaldívar, J., Padrón-Navarta, J.A., 2012. Late Variscan magmatism in the Nevado-Filábride Complex: U–Pb geochronologic evidence for the pre-Mesozoic nature of the deepest Betic complex (SE Spain). Lithos 146–147, 93–111.

Hack, J.T., 1957. Studies of longitudinal profiles in Virginia and Maryland. U. S. Geol. Surv. Prof. Pap. 294-B.

Harkins, N., Kirby, E., Heimsath, A., Robinson, R., Reiser, U., 2007. Transient fluvial incision in the headwaters of the Yellow River, northeastern Tibet, China. J. Geophys. Res. 112, F03S04. http://dx.doi.org/10.1029/2006JF000570.

Jabaloy, A., Galindo-Zaldívar, J., González-Lodeiro, F., 1992. The Mecina Extensional System: its relation with the post-Aquitanian piggy-back Basins and the paleostresses evolution (Betic Cordilleras, Spain). Geo-Mar. Lett. 12, 96–103.

Johnson, C., 1997. Resolving denudational histories in orogenic belts with apatite fission-track thermochronology and structural data: an example from southern Spain. Geology 25, 623–626.
Johnson, C., Harbury, N., Hurford, A., 1997. The role of extension in the Miocene denudation of the Nevado-Filábride Complex, Betic Cordillera (SE Spain). Tectonics 16, 189–204.
Keller, E.A., Pinter, N., 2002. Active Tectonics. second ed. Prentice Hall, New Jersey.
Kirby, E., Whipple, K.X., 2012. Expression of active tectonics in erosional landscapes. J. Struct. Geol. 44, 54–75.
Koulali, A., Ouazar, D., Tahayt, A., King, R.W., Vernant, P., Reilinger, R.E., McClusky, S., Mourabit, T., Davila, J.M., Amraoui, N., 2011. New GPS constraints on active deformation along the Africa–Iberia plate boundary. Earth Planet. Sci. Lett. 308, 211–217.
Larsen, I.J., Montgomery, D.R., 2012. Landslide erosion coupled to tectonics and river incision. Nat. Geosci. 5, 468–473. http://dx.doi.org/10.1038/ngeo1479.
Lonergan, L., 1993. Timing and kinematics of deformation in the Malaguide Complex, internal zone of the Betic Cordillera, southeast Spain. Tectonics 12, 460–476.
Lonergan, L., Platt, J.P., 1995. The Malaguide–Alpujarride boundary: a major extensional contact in the Internal Zone of the eastern Betic Cordillera, SE Spain. J. Struct. Geol. 17, 1655–1671.
Mancilla, F.d.L., Stich, D., Berrocoso, M., Martín, R., Morales, J., Fernández-Ros, A., Páez, R., Pérez-Peña, A., 2013. Delamination in the Betic Range: deep structure, seismicity, and GPS motion. Geology 41, 307–310.
Martínez-Martínez, J.M., 2006. Lateral interaction between metamorphic core complexes and less-extended, tilt-block domains: the Alpujarras strike-slip transfer fault zone (Betics, SE Spain). J. Struct. Geol. 28, 602–620. http://dx.doi.org/10.1016/j.jsg.2006.01.012.
Martínez-Martínez, J.M., Azañón, J.M., 1997. Mode of extensional tectonics in the southeastern Betics (SE Spain): Implications for the tectonic evolution of the peri-Alborán orogenic system. Tectonics 16, 205–225.
Martínez-Martínez, J.M., Soto, J.I., Balanyá, J.C., 2002. Orthogonal folding of extensional detachments: structure and origin of the Sierra Nevada elongated dome (Betics, SE Spain). Tectonics 21. http://dx.doi.org/10.1029/2001TC001283.
Martínez-Martínez, J.M., Soto, J.I., Balanyá, J.C., 2004. Special paper 380: gneiss domes in orogeny. Geol. Soc. Am. Spec. Pap. 380, 243–265.
Martínez-Martínez, J.M., Booth-Rea, G., Azañón, J.M., Torcal, F., 2006. Active transfer fault zone linking a segmented extensional system (Betics, southern Spain): insight into heterogeneous extension driven by edge delamination. Tectonophysics 422, 159–173.
Masana, E., Martínez-Díaz, J.J., Hernández-Enrile, J.L., Santanach, P., 2004. The Alhama de Murcia fault (SE Spain), a seismogenic fault in a diffuse plate boundary: seismotectonic implications for the Ibero–Magrebian region. J. Geophys. Res. B: Solid Earth 109, B01301.
Masek, J.G., Isacks, B.L., Gubbels, T.L., Fielding, E.J., 1994. Erosion and tectonics at the margins of continental plateaus. J. Geophys. Res. 99, 13,941–13,956.
Menéndez, I., Silva, P.G., Martín-Betancor, M., Pérez-Torrado, F.J., Guillou, H., Scaillet, S., 2008. Fluvial dissection, isostatic uplift, and geomorphological evolution of volcanic islands (Gran Canaria, Canary Islands, Spain). Geomorphology 102, 189–203.
Molin, P., Pazzaglia, F., Dramis, F., 2004. Geomorphic expression of active tectonics in a rapidly-deforming forearc, Sila massif, Calabria, southern Italy. Am. J. Sci. 304, 559–589.
Morales, J., Cantavella, J.V., de Lis Mancilla, F., Lozano, L., Stich, D., Herraiz, E., Martín, J.B., Lopez-Comino, J.A., Martinez-Solares, J.M., 2013. The 2011 Lorca seismic series: temporal evolution, faulting parameters and hypocentral relocation. Bull. Earthq. Eng. 12, 1871–1888.
Necea, D., Fielitz, W., Matenco, L., 2005. Late Pliocene–Quaternary tectonics in the frontal part of the SE Carpathians: insights from tectonic geomorphology. Tectonophysics 410, 137–156.
Pazzaglia, F.J., Brandon, M.T., 2001. A fluvial record of long-term steady-state uplift and erosion across the Cascadia forearc high, western Washington State. Am. J. Sci. 301, 385–431.
Pérez-Peña, J.V., Azañón, J.M., Azor, A., 2009a. CalHypso: an ArcGIS extension to calculate hypsometric curves and their statistical moments. Applications to drainage basin analysis in SE Spain. Comput. Geosci. 35, 1214–1223.
Pérez-Peña, J.V., Azañón, J.M., Azor, A., Tuccimei, P., Della Seta, M., Soligo, M., 2009b. Quaternary landscape evolution and erosion rates for an intramontane Neogene basin (Guadix–Baza basin, SE Spain). Geomorphology 106, 206–218.
Pérez-Peña, J.V., Azañón, J.M., Booth-Rea, G., Azor, A., Delgado, J., 2009c. Differentiating geology and tectonics using a spatial autocorrelation technique for the hypsometric integral. J. Geophys. Res. 114, F02018.
Pérez-Peña, J., Azor, A., Azañón, J., Keller, E., 2010. Active tectonics in the Sierra Nevada (Betic Cordillera, SE Spain): insights from geomorphic indexes and drainage pattern analysis. Geomorphology 119, 74–87.
Platt, J.P., Vissers, R.L.M., 1989. Extensional collapse of thickened continental lithosphere: a working hypothesis for the Alboran Sea and Gibraltar arc. Geology 17, 540.
Platt, J.P., Kelley, S.P., Carter, A., Orozco, M., 2005. Timing of tectonic events in the Alpujárride Complex, Betic Cordillera, southern Spain. J. Geol. Soc. Lond. 162, 1–12.
Platt, J.P., Anczkiewicz, R., Soto, J.-I., Kelley, S.P., Thirlwall, M., 2006. Early Miocene continental subduction and rapid exhumation in the western Mediterranean. Geology 34, 981.
Platt, J.P., Behr, W.M., Johanesen, K., Williams, J.R., 2013. The Betic–Rif Arc and its orogenic hinterland: a review. Annu. Rev. Earth Planet. Sci. 41, 313–357.
Reinhardt, L.J., Dempster, T.J., Shroder, J.F., Persano, C., 2007. Tectonic denudation and topographic development in the Spanish Sierra Nevada. Tectonics 26, TC3001.
Rodríguez-Fernández, J., Sanz de Galdeano, C., 2006. Late orogenic intramontane basin development: the Granada basin, Betics (southern Spain). Basin Res. 18, 85–102.
Rodríguez-Fernández, J., Azor, A., Miguel Azañón, J., 2012. The Betic Intramontane Basins (SE Spain): Stratigraphy, Subsidence, and Tectonic History. Tectonics of Sedimentary Basins. John Wiley & Sons Ltd., pp. 461–479.
Sánchez-Vizcaíno, V., López Rubatto, D., Gómez-Pugnaire, M.T., Trommsdorff, V., Müntener, O., 2002. Middle Miocene high-pressure metamorphism and fast exhumation of the Nevado-Filábride Complex, SE Spain. Terra Nova 13, 327–332.
Sanz de Galdeano, C., 1996. The E–W segments of the contact between the external and internal zones of the Betic and Rif cordilleras and the E–W corridors of the internal zone (a combined explanation). Estud. Geol. 52, 123–136.
Sanz de Galdeano, C., García-Tortosa, F.J., Peláez, J.A., Alfaro, P., Azañón, J.M., Galindo-Zaldívar, J., López Casado, C., López Garrido, A.C., Rodríguez-Fernández, J., Ruano, P., 2012. Main active faults in the Granada and Guadix–Baza Basins (Betic Cordillera). J. Iber. Geol. 38, 209–223.
Scotti, V.N., Molin, P., Faccenna, C., Soligo, M., Casas-Sainz, A., 2014. The influence of surface and tectonic processes on landscape evolution of the Iberian Chain (Spain): quantitative geomorphological analysis and geochronology. Geomorphology 206, 37–57.
Siddiqui, S., Soldati, M., 2014. Appraisal of active tectonics using DEM-based hypsometric integral and trend surface analysis in Emilia-Romagna Apennines, northern Italy. Turk. J. Earth Sci. 23, 277–292.
Strahler, A.N., 1952. Hypsometric (area-altitude) analysis of erosional topography. Geol. Soc. Am. Bull. 63, 1117–1142.
Van der Beek, P., Braun, J., 1998. Numerical modeling of landscape evolution on geological time-scales: a parameter analysis and comparison with the south-eastern highlands of Australia. Basin Res. 10, 49–68.
van der Beek, P., Champel, B., Mugnier, J.-L., 2002. Control of detachment dip on drainage development in regions of active fault-propagation folding. Geology 30, 471–474.
Vázquez, M., Jabaloy, A., Barbero, L., Stuart, F., 2011. Deciphering tectonic and erosion-driven exhumation of the Nevado–Filábride Complex (Betic Cordillera, Southern Spain) by low temperature thermochronology. Terra Nova 23, 257–263.
Viseras, C., Calvache, M., Soria, J., Fernández, J., 2003. Differential features of alluvial fans controlled by tectonic or eustatic accommodation space. Examples from the Betic Cordillera, Spain. Geomorphology 50, 181–202.
Visser, S.M., Platt, J.P., Van der Wal, D., 1995. Late orogenic extension of the Betic Cordillera and the Alboran Domain: a lithospheric view. Tectonics 14, 786–803.
Watts, A.B., Platt, J.P., Bulh, P., 1993. Tectonic evolution of the Alboran Sea basin. Basin Res. 5, 153–177.
Wegmann, K.W., Pazzaglia, F.J., 2002. Holocene strath terraces, climate change, and active tectonics: the Clearwater River basin, Olympic Peninsula, Washington State. Geol. Soc. Am. Bull. 114, 731–744.
Whipple, K.X., 2001. Fluvial landscape response time: how plausible is steady-state denudation? Am. J. Sci. 301, 313–325.
Whipple, K.X., 2004. Bedrock rivers and the geomorphology of active orogens. Annu. Rev. Earth Planet. Sci. 32, 151–185.
Whipple, K.X., DiBiase, R.A., Crosby, B.T., 2013. Bedrocks rivers. In: Shroder, J.F. (Ed.), Treatise on Geomorphology. Elsevier, Poland, pp. 550–573.
Whittaker, A.C., Cowie, P.A., Attal, M., Tucker, G.E., Roberts, G.P., 2007. Contrasting transient and steady-state rivers crossing active normal faults: new field observations from the Central Apennines, Italy. Basin Res. 19 (4), 529–556.
Willgoose, G., Hancock, G., 1998. Revisiting the hypsometric curve as an indicator of form and process in transport-limited catchment. Earth Surf. Process. Landf. 23, 611–623.
Wittmann, H., von Blanckenburg, F., Kruesmann, T., Norton, K.P., Kubik, P.W., 2007. Relation between rock uplift and denudation from cosmogenic nuclides in river sediment in the Central Alps of Switzerland. J. Geophys. Res. 112, F04010.
Wobus, C., Whipple, K.X., Kirby, E., Synder, N., Johnson, J., Spyropolou, K., Crosby, B., Sheehan, D., 2006. Tectonics from topography: procedures, promise, and pitfalls. In: Willett, S.D., Hovius, N., Brandon, M.T., Fisher, D.M. (Eds.), Tectonics, Climate and Landscape Evolution. Geology Society of America Spatial Papers, pp. 55–74.
Zhang, K., Liu, K., Yang, J., 2004. Asymmetrical valleys created by the geomorphic response of rivers to strike-slip fault. Quat. Res. 62, 310–315.